

# 4DVGGT-D: 4D Visual Geometry Transformer with Improved Dynamic Depth Estimation

Ying Zang<sup>4,\*</sup>, Xuanyi Liu<sup>2,\*</sup>, Yidong Han<sup>4,\*</sup>, Deyi Ji<sup>1</sup>, Chaotao Ding<sup>1</sup>, Yuanqi Hu<sup>1</sup>, Qi Zhu<sup>5</sup>, Xuanfu Li<sup>6</sup>, Jin Ma<sup>6</sup>, Lingyun Sun<sup>3</sup>, Tianrun Chen<sup>1,3,†</sup>, Lanyun Zhu<sup>7</sup>

<sup>1</sup>KOKONI 3D, Moxin Technology, <sup>2</sup>Peking University, <sup>3</sup>Zhejiang University, <sup>4</sup>Huzhou University, <sup>5</sup>Univeristy of Science and Technology of China, <sup>6</sup>Huawei, <sup>7</sup>Tongji University

\*Equal Contribution, †Project Lead

## Abstract

Reconstructing dynamic 4D scenes from monocular videos is a fundamental yet challenging task. While recent 3D foundation models provide strong geometric priors, their performance significantly degrades in dynamic environments. This degradation stems from a fundamental tension: the inherent coupling of camera ego-motion and object motion within global attention mechanisms. In this paper, we propose a novel, training-free progressive decoupling framework that disentangles dynamics from statics in a principled, coarse-to-fine manner. Our core insight is to resolve the tension by first stabilizing the camera pose, followed by geometric refinement. Specifically, our approach consists of three synergistic components: (1) a *Dynamic-Mask-Guided Pose Decoupling* module that isolates pose estimation from dynamic interference, yielding a stable motion-free reference frame; (2) a *Topological Subspace Surgery* mechanism that orthogonally decomposes the depth manifold, safely preserving dynamic objects while injecting refined, mask-aware geometry into static regions; and (3) an *Information-Theoretic Confidence-Aware Fusion* strategy that formulates depth integration as a heteroscedastic Bayesian inference problem, adaptively blending multi-pass predictions via inverse-variance weighting. Extensive experiments on standard 4D reconstruction benchmarks demonstrate that our method achieves consistent and substantial improvements across principal point-cloud metrics. Notably, our approach shows competitive performance in robust 4D scene reconstruction without requiring fine-tuning, suggesting the potential of mathematically grounded dynamic-static disentanglement.

**Correspondence:** Deyi Ji, Tianrun Chen, Lanyun Zhu

## 1 Introduction

Despite recent advances in feedforward 3D estimation of static scenes from image sets [13, 20, 22], extending these remarkable capabilities to dynamic environments, scenes where objects or people undergo motion or deformation, remains a significant challenge. In particular, the Visual Geometry Grounded Transformer (VGGT)[20] has emerged as a cornerstone in this domain. By leveraging a unified transformer architecture that jointly predicts camera poses, depth maps, and point correspondences via alternating intra-frame and cross-frame global attention, VGGT achieves unprecedented zero-shot generalization in static environments.

<sup>1</sup>We thank Jianyuan Wang for his insightful discussions. We acknowledge the support from Hisilicon, the ZJU Kungpeng & Ascend Center of Excellence, and the Dream Set Off - Kungpeng & Ascend Seed Program.

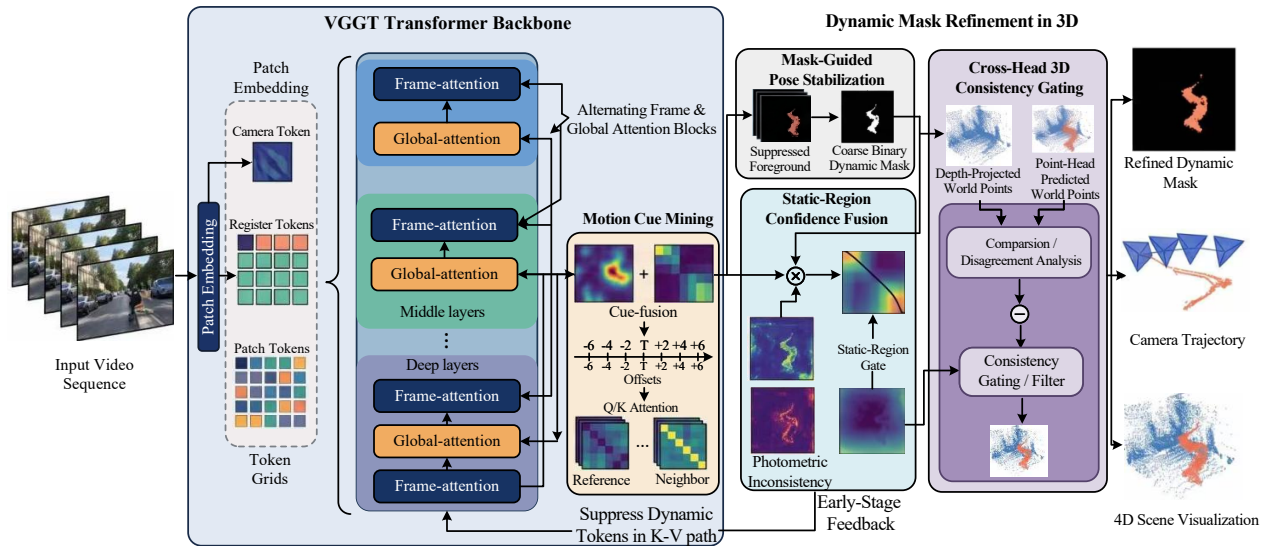


**Figure 1** Overview of the proposed progressive decoupling framework. Given an input video sequence, the VGGT backbone extracts features while the Motion Cue Mining module generates an initial dynamic mask. To resolve the tension between pose and geometry, the Mask-Guided Pose Stabilization module filters dynamic tokens to establish a motion-free static reference frame. Subsequently, Topological Subspace Surgery and Static-Region Confidence Fusion adaptively blend multi-pass depth predictions based on heteroscedastic uncertainty, yielding a refined dynamic mask and robust 4D scene reconstruction.

While VGGT demonstrates strong performance in static scene understanding, its accuracy drops significantly when applied to dynamic environments. This limitation stems from a fundamental tension: motion provides valuable cues for geometry estimation in dynamic scenarios, yet simultaneously introduces noise that corrupts camera pose estimation by violating the static epipolar constraint[30]. In other words, the very signals that enable reconstructing dynamic objects are also those that hinder reliable pose recovery.

A common strategy for handling such dynamic scenarios is to decompose the problem into a series of sub-modules, such as depth estimation, optical flow computation, and object tracking [7, 11? ]. While this modular approach simplifies the task by disentangling different components, it often results in increased computational cost and error accumulation across sequential stages. Given the limitations of modular pipelines, developing unified methods offers a more effective solution. Yet, creating such models typically requires capturing complex spatiotemporal relationships across frames and demands notable computational resources as well as access to large-scale dynamic datasets with ground-truth geometry [21, 24]. Recent adaptations like VGGT4D [8] attempt to mitigate this by mining motion cues directly from pretrained attention layers without fine-tuning. However, a more principled, multi-stage decoupling is required to fully resolve the geometric conflicts in 4D scenes.

Motivated by these challenges, we present a unified and efficient training-free framework for robust 4D scene reconstruction. To address the limited availability of labeled dynamic data and the high cost of optimization, we build on the pretrained 3D foundation model VGGT and adapt it to dynamic scenarios without any fine-tuning. Recognizing the inherent conflict between pose and geometry, our central idea is to explicitly disentangle their effects. Rather than attempting to correct both in a single pass, we propose a progressive decoupling approach guided by a simple yet powerful philosophy: *first stabilize the camera, then stabilize the geometry*.

To achieve this, we first introduce a Dynamic-Mask-Guided Pose Decoupling module. This step identifies dynamic regions and filters them out using a key-suppression mechanism. By strictly preventing dynamic content from polluting the global context, we deliberately prioritize global trajectory consistency over local relative smoothness. This conscious trade-off successfully yields a motion-free Riemannian reference frame that serves as a vastly superior foundation for dense 3D geometry. Once the camera is stabilized, we shift our

focus to refining the scene geometry. To optimally integrate multi-pass predictions, we employ a Topological Subspace Surgery mechanism alongside an Information-Theoretic Confidence-Aware Fusion strategy. This principled design allows us to harness mask-aware geometry where it benefits static background grounding, while conservatively preserving the structural integrity of dynamic pixels. With this progressive formulation, our method achieves accurate pose and geometry estimation for both static and dynamic content in challenging scenarios.

Through extensive experiments, our progressive decoupling framework establishes new state-of-the-art performance across multiple point-cloud metrics on the DyCheck benchmark. For instance, compared to the strong VGGT4D baseline [8], it reduces the Distance Mean from 0.0646 to 0.0516 and improves the Completeness Mean from 0.0962 to 0.0751. Notably, thanks to its training-free, plug-in design, our approach adds only a negligible overhead in runtime compared to the base model. This work makes the following key contributions:

- We propose a training-free, progressive decoupling framework for robust 4D scene reconstruction, which achieves state-of-the-art results on dynamic geometry perception benchmarks without requiring any fine-tuning.
- We introduce a **Dynamic-Mask-Guided Pose Decoupling** module that explicitly disentangles pose estimation from dynamic interference. By projecting the camera estimation onto a motion-free Riemannian submanifold of  $SE(3)$ , it anchors a globally consistent static reference frame for subsequent geometric refinement.
- We design a **Topological Subspace Surgery** mechanism and an **Information-Theoretic Confidence-Aware Fusion** strategy. By formulating depth integration as a heteroscedastic Bayesian inference problem, our method adaptively blends multi-pass predictions via inverse-variance weighting, maximizing geometric fidelity for both static and dynamic regions.

## 2 Related Work

**3D Foundation Models.** The advent of feed-forward 3D foundation models has significantly accelerated pose-free dense reconstruction. DUST3R [22] pioneered this paradigm by predicting dense pointmaps from image pairs via pairwise cross-attention. MAST3R [13] strengthened correspondence quality, and Reloc3R [4] directly regressed 6-DoF poses for sharper camera estimation. However, pairwise inputs make inference cost grow quadratically with sequence length. To lift this constraint, multi-image variants introduce memory encoders [2, 19] and subgraph fusion [15] to aggregate context without exhaustive pairing. VGGT [20] and Fast3R [25] further employ global attention for cross-view reasoning, while MV-DUST3R+ [18] couples such priors with 3D Gaussian Splatting [10] for end-to-end reconstruction from sparse views. Recent follow-ups push beyond these methods with unified dense-geometry prediction [5], causal streaming for long sequences [12], and training-free token-merging acceleration [17]. Despite their success, these models are predominantly trained under static-scene assumptions and lack an explicit mechanism to disentangle moving objects.

**4D Scene Reconstruction.** Traditional 4D reconstruction methods often rely on joint optimization of depth, pose, and residual motion, utilizing self-supervised photometric losses or test-time bundle adjustment (e.g., Robust-CVD [11], CasualSAM [29]). More recent pipelines such as MegaSaM [14] achieve robust poses by leveraging strong monocular depth priors, while Uni4D [26] integrates multiple visual foundation models with multi-stage bundle adjustment. These approaches are effective but hinge on heavy test-time optimization, which limits scalability. Recent learning-based approaches aim to reduce optimization overhead: MonST3R [27] fine-tunes on dynamic data and leverages optical flow priors; DAS3R [24] augments a DPT head for feed-forward motion masking; CUT3R [21] fine-tunes MAST3R on mixed static/dynamic data; PAGE-4D [30] introduces a dynamics-aware aggregator to explicitly disentangle pose and geometry estimation; Easi3R [3] proposes a training-free adaptation for DUST3R by analyzing attention statistics, but its pairwise nature limits temporal consistency. SpatialTrackerV2 [23] and POMATO [28] explore efficient feed-forward architectures but still require training on dynamic datasets. Our work builds upon the insight that global attention inherently encodes motion, but we fundamentally differ by proposing a multi-stage, progressive decoupling mechanism that explicitly isolates pose estimation from geometric refinement, achieving superior results without any fine-tuning.

**Uncertainty-Aware Depth Estimation.** Modeling uncertainty in depth prediction has been explored in both monocular [9, 16] and multi-view settings [1]. These works typically predict a per-pixel variance alongside depth, enabling downstream tasks to weight predictions by their reliability. Our confidence-aware fusion extends this principle to the multi-pass setting, where two depth estimates with distinct noise characteristics must be optimally combined.

### 3 Method

Given a monocular video sequence  $\mathcal{X} = \{I_t\}_{t=1}^N$  containing dynamic objects, our goal is to estimate the camera extrinsics  $\{E_t\}_{t=1}^N$  and reconstruct a dense 4D point cloud. We build upon a pretrained 3D foundation model  $\Phi_\theta$ , and adapt it to dynamic scenes without fine-tuning.

Our framework performs two forward passes. The first pass applies the original model to obtain initial depth maps  $\mathcal{D}^{(1)}$ , confidence maps  $\mathcal{C}^{(1)}$ , camera poses, and attention-derived dynamic masks. The second pass suppresses dynamic tokens in early attention layers and produces pose-stabilized extrinsics  $\tilde{E}$ , depth maps  $\tilde{\mathcal{D}}$ , and confidence maps  $\tilde{\mathcal{C}}$ . Finally, we preserve the first-pass depth in dynamic regions and fuse the two depth estimates in static regions according to confidence. The overall design follows a simple principle: first reduce dynamic interference for camera estimation, then refine geometry using both passes.

#### 3.1 Preliminary: VGGT and Attention-Based Dynamic Cues

Our framework is instantiated on the Visual Geometry Grounded Transformer (VGGT) [20], a pretrained 3D foundation model that jointly predicts camera poses, depth maps, and point correspondences. VGGT flattens input images into token sequences and processes them with alternating intra-frame and cross-frame global attention layers. This design is effective for static scenes, but in dynamic scenes the same global attention can mix camera ego-motion with object motion, leading to inaccurate pose and geometry estimates.

Following recent training-free adaptations such as VGGT4D [8], we extract dynamic cues from the pretrained attention layers. Let  $\mathbf{Q}_l, \mathbf{K}_l \in \mathbb{R}^{N_{\text{tok}} \times d}$  denote the query and key matrices at layer  $l$ . For a reference frame  $r$  and a source frame  $s$ , we compute the normalized Gram similarities:

$$\mathbf{G}_{l,r,s}^{QQ} = \frac{\mathbf{Q}_{l,r} \mathbf{Q}_{l,s}^\top}{\|\mathbf{Q}_{l,r}\| \|\mathbf{Q}_{l,s}\|}, \quad \mathbf{G}_{l,r,s}^{KK} = \frac{\mathbf{K}_{l,r} \mathbf{K}_{l,s}^\top}{\|\mathbf{K}_{l,r}\| \|\mathbf{K}_{l,s}\|}. \quad (1)$$

These similarities are aggregated across selected layers and temporal neighbors to produce an initial dynamic saliency map  $\mathcal{M}_{\text{dyn}} \in [0, 1]^{H \times W}$ . Pixels with high saliency are likely to belong to independently moving regions. We use this mask not as a final segmentation result, but as a cue for separating pose estimation from dynamic geometry reconstruction.

#### 3.2 Pose--Geometry Conflict in Dynamic Scenes

We first describe the conflict caused by object motion. Under the standard static-scene assumption, the correspondence between a reference pixel  $\mathbf{x}_r$  and a target pixel  $\mathbf{x}_t$  is determined by the camera intrinsics  $\mathbf{K}$ , reference depth  $D_r(\mathbf{x}_r)$ , and relative pose  $[\mathbf{R}_{t \leftarrow r} \mid \mathbf{t}_{t \leftarrow r}]$ :

$$\mathbf{x}_t = \mathbf{K} [\mathbf{R}_{t \leftarrow r} D_r(\mathbf{x}_r) \mathbf{K}^{-1} \mathbf{x}_r + \mathbf{t}_{t \leftarrow r}]. \quad (2)$$

This leads to the epipolar constraint:

$$\tilde{\mathbf{x}}_t^\top \mathbf{E} \tilde{\mathbf{x}}_r = 0, \quad \mathbf{E} = [\mathbf{t}_{t \leftarrow r}]_\times \mathbf{R}_{t \leftarrow r}, \quad (3)$$

where  $\tilde{\mathbf{x}}_r$  and  $\tilde{\mathbf{x}}_t$  are homogeneous pixel coordinates.

In a dynamic scene, an independently moving point introduces an additional displacement term. A simplified correspondence can be written as:

$$\mathbf{x}_t = \mathbf{K} [\mathbf{R}_{t \leftarrow r} D_r(\mathbf{x}_r) \mathbf{K}^{-1} \mathbf{x}_r + \mathbf{t}_{t \leftarrow r} + \Delta \mathbf{X}_{t \leftarrow r}(\mathbf{x}_r)], \quad (4)$$

where  $\Delta\mathbf{X}_{t\leftarrow r}$  denotes the 3D displacement caused by object motion. This displacement violates the static epipolar constraint and produces a non-zero residual:

$$\delta(\mathbf{x}_r) \equiv \tilde{\mathbf{x}}_t^\top \mathbf{E} \tilde{\mathbf{x}}_r \approx \frac{1}{Z_r} \mathbf{n}(\mathbf{x}_r)^\top \Delta\mathbf{X}_\perp(\mathbf{x}_r), \quad (5)$$

where  $\mathbf{n}(\mathbf{x}_r)$  is the unit normal of the epipolar line and  $\Delta\mathbf{X}_\perp$  is the component of the dynamic displacement perpendicular to that line [30].

This creates a practical tension. Camera pose estimation benefits from suppressing dynamic regions because they violate static correspondence assumptions. In contrast, geometry reconstruction should preserve dynamic regions because they are part of the target 4D scene. Treating both objectives in a single unmodified forward pass can therefore mix two incompatible signals. Our method addresses this by first estimating a more stable camera frame from static regions, and then reconstructing geometry with a region-aware fusion strategy.

### 3.3 Dynamic-Mask-Guided Pose Decoupling

Let  $\mathcal{T} = \{T_t\}_{t=1}^N$  denote the camera-to-world transformations, with each  $T_t \in SE(3)$ . In a standard dense correspondence formulation, pose estimation can be viewed as minimizing a global geometric loss:

$$\mathcal{T}^* = \arg \min_{\mathcal{T} \in SE(3)^N} \sum_{t=1}^N \int_{\Omega} \mathcal{L}_{\text{geo}}(\mathbf{p}, T_t) d\mathbf{p}, \quad (6)$$

where  $\Omega$  is the image domain. In dynamic scenes, pixels on moving objects contribute motion-inconsistent correspondences to this objective. Ideally, pose estimation should rely more on static regions:

$$\mathcal{J}(\mathcal{T}) = \sum_{t=1}^N \int_{\Omega} (1 - \mathcal{M}_{\text{dyn}}(\mathbf{p})) \mathcal{L}_{\text{geo}}(\mathbf{p}, T_t) d\mathbf{p}. \quad (7)$$

Instead of solving Eq. equation 7 through test-time optimization, we approximate this static-region bias with a mask-aware forward pass. Specifically, for early attention layers, we suppress the key vectors of tokens predicted as dynamic:

$$\hat{\mathbf{K}}_l(\mathbf{p}) = \begin{cases} \mathbf{0}, & \mathcal{M}_{\text{dyn}}(\mathbf{p}) \geq \tau \text{ and } l \leq L_{\text{mask}}, \\ \mathbf{K}_l(\mathbf{p}), & \text{otherwise.} \end{cases} \quad (8)$$

Here,  $\tau$  is the dynamic-mask threshold and  $L_{\text{mask}}$  controls the number of early layers where suppression is applied. This operation reduces the influence of dynamic regions when global context is aggregated, making the predicted camera trajectory more dependent on static correspondences.

The mask-aware pass outputs pose-stabilized extrinsics  $\tilde{E} = \{\tilde{E}_t\}_{t=1}^N$ , depth maps  $\tilde{D} = \{\tilde{D}_t\}_{t=1}^N$ , and confidence maps  $\tilde{C} = \{\tilde{C}_t\}_{t=1}^N$ . We use  $\tilde{E}$  as the camera reference for the subsequent reconstruction stage. However, since dynamic tokens are suppressed in this pass, its depth predictions in moving regions may be less reliable. This motivates the region-aware depth construction below.

### 3.4 Region-Aware Depth Construction

A simple solution would be to directly adopt the mask-aware depth  $\tilde{D}$ . This is undesirable because the second pass is optimized for pose stabilization and suppresses dynamic tokens. As a result, its predictions in moving regions can lose object details. We therefore combine the two passes according to the dynamic mask.

We define the static and dynamic regions as:

$$\mathcal{S} = \{\mathbf{p} \in \Omega \mid \mathcal{M}_{\text{dyn}}(\mathbf{p}) < \tau\}, \quad \mathcal{D}_{\text{dyn}} = \Omega \setminus \mathcal{S}. \quad (9)$$

Let  $\Pi_{\mathcal{S}}$  and  $\Pi_{\mathcal{D}_{\text{dyn}}}$  denote restriction operators that keep values only in the corresponding regions. Since these two regions have disjoint support, the depth map can be decomposed into static and dynamic parts:

$$\mathcal{D}_{3a} = \Pi_{\mathcal{D}_{\text{dyn}}} \mathcal{D}^{(1)} + \Pi_{\mathcal{S}} \tilde{D}. \quad (10)$$

Equivalently, at each pixel:

$$\mathcal{D}_{3a}(\mathbf{p}) = \mathbb{1}_{\mathcal{D}_{\text{dyn}}}(\mathbf{p})\mathcal{D}^{(1)}(\mathbf{p}) + \mathbb{1}_{\mathcal{S}}(\mathbf{p})\tilde{\mathcal{D}}(\mathbf{p}). \quad (11)$$

This construction preserves the first-pass geometry in dynamic regions while using the pose-stabilized prediction in static regions. It provides a simple region-aware baseline, but the hard boundary may introduce discontinuities near object borders and may propagate local errors from the second pass inside static regions. We address this with confidence-aware fusion.

### 3.5 Confidence-Aware Depth Fusion

We further refine the static-region depth by fusing the two predictions according to their confidence. At each pixel, we model the two depth estimates as noisy observations of the same latent depth  $d^*(\mathbf{p})$ :

$$\mathcal{D}^{(i)}(\mathbf{p}) = d^*(\mathbf{p}) + \epsilon_i(\mathbf{p}), \quad \epsilon_i(\mathbf{p}) \sim \mathcal{N}(0, \sigma_i^2(\mathbf{p})), \quad i \in \{1, 2\}, \quad (12)$$

where  $\mathcal{D}^{(2)} = \tilde{\mathcal{D}}$ . We interpret the confidence maps as proportional to inverse variance:

$$\sigma_1^{-2}(\mathbf{p}) \propto \mathcal{C}^{(1)}(\mathbf{p}), \quad \sigma_2^{-2}(\mathbf{p}) \propto \tilde{\mathcal{C}}(\mathbf{p}). \quad (13)$$

Assuming the two observations are conditionally independent given  $d^*(\mathbf{p})$ , the maximum-likelihood estimate is obtained by minimizing the weighted squared error:

$$\hat{d}(\mathbf{p}) = \arg \min_d \sum_{i=1}^2 \frac{(d - \mathcal{D}^{(i)}(\mathbf{p}))^2}{2\sigma_i^2(\mathbf{p})}. \quad (14)$$

This gives the inverse-variance weighted estimator:

$$\hat{d}(\mathbf{p}) = \frac{\sigma_1^{-2}(\mathbf{p})\mathcal{D}^{(1)}(\mathbf{p}) + \sigma_2^{-2}(\mathbf{p})\tilde{\mathcal{D}}(\mathbf{p})}{\sigma_1^{-2}(\mathbf{p}) + \sigma_2^{-2}(\mathbf{p})}. \quad (15)$$

Using confidence as precision, this can be written as:

$$\hat{d}(\mathbf{p}) = (1 - \mathcal{W}(\mathbf{p}))\mathcal{D}^{(1)}(\mathbf{p}) + \mathcal{W}(\mathbf{p})\tilde{\mathcal{D}}(\mathbf{p}), \quad (16)$$

where

$$\mathcal{W}(\mathbf{p}) = \frac{\tilde{\mathcal{C}}(\mathbf{p})}{\mathcal{C}^{(1)}(\mathbf{p}) + \tilde{\mathcal{C}}(\mathbf{p}) + \epsilon}. \quad (17)$$

Here,  $\epsilon$  is a small constant for numerical stability. The weight  $\mathcal{W}$  increases when the mask-aware pass is more confident and decreases when the first pass is more reliable.

The final depth is defined by applying confidence-aware fusion in the static region and preserving the first-pass depth in the dynamic region:

$$\mathcal{D}_{3b}(\mathbf{p}) = \begin{cases} \mathcal{D}^{(1)}(\mathbf{p}), & \mathbf{p} \in \mathcal{D}_{\text{dyn}}, \\ (1 - \mathcal{W}(\mathbf{p}))\mathcal{D}^{(1)}(\mathbf{p}) + \mathcal{W}(\mathbf{p})\tilde{\mathcal{D}}(\mathbf{p}), & \mathbf{p} \in \mathcal{S}. \end{cases} \quad (18)$$

This fusion can also be interpreted through Fisher information. For a Gaussian observation with variance  $\sigma^2$ , the Fisher information with respect to the mean is  $\sigma^{-2}$ . Therefore, Eq. equation 15 weights each depth estimate according to its relative information under the Gaussian noise model. Under the conditional-independence approximation, the fused precision is:

$$\sigma_{\text{fused}}^{-2}(\mathbf{p}) = \sigma_1^{-2}(\mathbf{p}) + \sigma_2^{-2}(\mathbf{p}) \propto \mathcal{C}^{(1)}(\mathbf{p}) + \tilde{\mathcal{C}}(\mathbf{p}). \quad (19)$$

This suggests that the fused estimate can reduce posterior uncertainty when the confidence maps are well calibrated.

**Table 1 Quantitative comparison on the DyCheck dataset.** We report point cloud reconstruction metrics (Accuracy, Completeness, Distance) and camera pose estimation metrics (ATE, RTE, RRE). All metrics are distance-based (lower is better). Our method achieves the best performance on principal point cloud geometric metrics, demonstrating the effectiveness of our progressive decoupling framework.

Method	Accuracy ↓		Completeness ↓		Distance ↓		Pose Estimation		
	Mean	Med.	Mean	Med.	Mean	Med.	ATE ↓	RTE ↓	RRE ↓
Easi3R <sub>DUST3R</sub> [3]	0.0700	0.0440	0.0600	0.0330	0.1940	0.1320	0.0220	0.0090	0.8060
Easi3R <sub>MonST3R</sub> [3]	0.1000	0.0500	0.1210	0.0820	0.2890	0.2700	0.0320	<b>0.0080</b>	1.0750
MonST3R [27]	0.0900	0.0330	0.1130	0.0640	0.2790	0.2340	0.0380	0.0100	1.1720
POMATO [28]	0.9600	0.9500	0.8140	0.7760	1.4840	1.4340	0.1280	0.0270	3.6480
SpatialTrackerV2 [23]	0.1150	0.0640	0.0520	0.0260	0.4210	0.3040	<b>0.0110</b>	0.0060	0.3470
DAS3R [24]	0.1920	0.1420	0.2500	0.1080	0.4280	0.3360	0.0520	0.0120	1.5600
CUT3R [21]	0.0730	0.0540	0.1330	0.0490	0.3280	0.2240	0.0360	0.0130	0.8600
Baseline (VGGT4D) [8]	0.0331	0.0222	0.0962	0.0628	0.0646	0.0425	0.0183	0.0100	<b>0.3450</b>
<b>Ours</b>	<b>0.0280</b>	<b>0.0188</b>	<b>0.0751</b>	<b>0.0528</b>	<b>0.0516</b>	<b>0.0358</b>	0.0142	0.0114	0.4406

## 4 Experiments

### 4.1 Experimental Setup

**Datasets and Metrics.** Following the evaluation protocol established by prior work [6, 8], we assess our method on the DyCheck [6] dataset, which provides challenging dynamic sequences with ground-truth point clouds and camera trajectories. To comprehensively evaluate the quality of the 4D reconstruction, we employ the standard 3D point cloud metrics: Accuracy (Mean and Median), Completeness (Mean and Median), and Distance (Mean and Median), all of which are distance-based (lower is better). We also report Absolute Trajectory Error (ATE), Relative Translation Error (RTE), and Relative Rotation Error (RRE) for camera pose evaluation.

**Baselines.** We compare against a comprehensive set of state-of-the-art methods, including Easi3R [3], MonST3R [27], DAS3R [24], CUT3R [21], SpatialTrackerV2 [23], POMATO [28], and our primary baseline VGGT4D [8].

**Implementation Details.** We use the pretrained VGGT model as the backbone without any fine-tuning. The masking depth  $L_{\text{mask}}$  is set to 5, and the dynamic threshold  $\tau$  is determined via Otsu’s algorithm. The regularization constant  $\epsilon$  is set to  $10^{-6}$ .

### 4.2 Comparison with State-of-the-Art Methods

Table 1 presents a comprehensive comparison with state-of-the-art methods on the DyCheck dataset. Our method achieves the best performance across the principal point cloud reconstruction geometric metrics. Compared to our strong baseline (VGGT4D), we reduce the Accuracy Mean by 15.4% ( $0.0331 \rightarrow 0.0280$ ), Completeness Mean by 21.9% ( $0.0962 \rightarrow 0.0751$ ), and Distance Mean by 20.1% ( $0.0646 \rightarrow 0.0516$ ).

We explicitly acknowledge that while our method significantly improves the geometric fidelity of the reconstructed 3D point cloud, it does not achieve universal monotonicity across all pose metrics. Specifically, the Relative Translation Error (RTE) and Relative Rotation Error (RRE) exhibit variance and degradation compared to the baseline. This aligns with the fundamental tension discussed in Section 3.2: fully decoupling dynamics to stabilize the background geometry can involve trade-offs in continuous pose tracking. However, since the ultimate goal of dense 4D reconstruction is the structural integrity of the scene, the substantial enhancement in point cloud geometry validates our progressive decoupling approach.

To provide a more intuitive understanding of our performance improvements, we present qualitative comparisons in and Figure 2 and Figure 3 .



**Figure 2** Qualitative comparison of dynamic region tracking and scene reconstruction on the DyCheck dataset. Compared to state-of-the-art methods such as DAS3R, Easi3R, MonSTR3R, and the VGGT4D baseline, our approach more accurately isolates dynamic objects from the static background. Red boxes highlight areas where our progressive decoupling effectively reduces motion artifacts and preserves the structural integrity of complex dynamic entities.

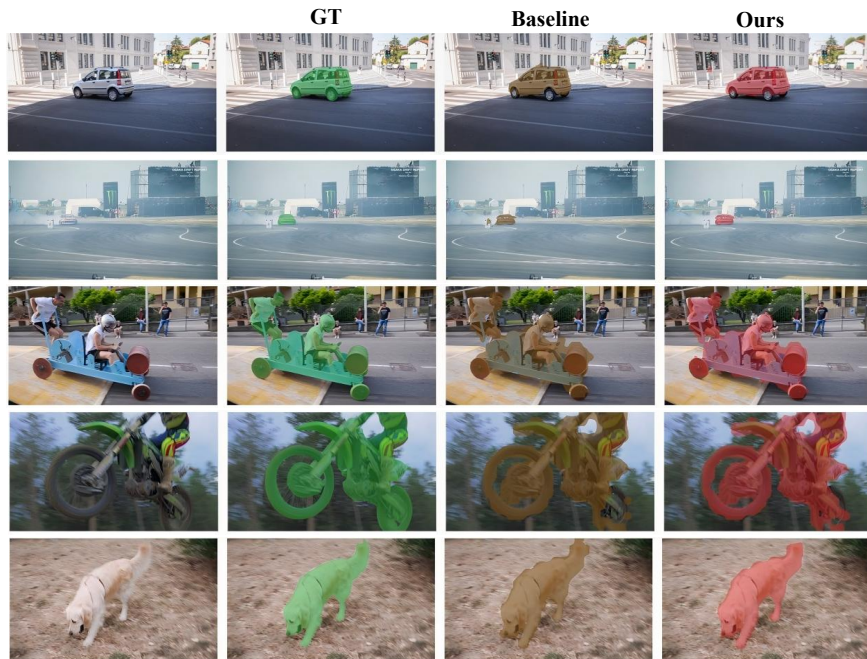


**Figure 3** Visual comparison of reconstructed scene geometry. We compare the ground truth (GT) geometry against the baseline and our proposed method. By explicitly disentangling statics from dynamics, our approach effectively suppresses dynamic noise and recovers more complete and accurate object structures that closely match the ground truth references.

Figure 2 further highlights the geometric fidelity of our reconstructions compared to the VGGT4D baseline and the ground truth. The baseline method exhibits noticeable distortions around moving elements because its global attention mechanism inherently couples object motion with camera ego-motion. Our approach mitigates this issue through topological subspace surgery and confidence-aware fusion. As demonstrated in the visualizations, our method not only recovers sharp and accurate boundaries for dynamic objects but also maintains a smooth and continuous representation of the static background. This visual evidence strongly aligns with our quantitative gains and confirms the robustness of our mathematical formulation for dynamic and static disentanglement.

Figure 3 illustrates the dynamic region segmentation and scene visualization across multiple challenging sequences. State-of-the-art baselines often struggle with severe motion interference, leading to incomplete object boundaries and noisy background artifacts. In contrast, our progressive decoupling framework effectively isolates dynamic entities. By establishing a stable static reference frame, our method prevents moving objects from corrupting the surrounding geometry.

### 4.3 Ablation Study

**Impact of Pose Decoupling.** Implementing the mask-guided pose decoupling alone yields the most significant geometric improvement, reducing the Accuracy Mean by 14.8%, Completeness Mean by 19.0%, and Distance Mean by 17.8%. Furthermore, this module improves the global Absolute Trajectory Error (ATE) by 22.4%. However, we observe an increase in Relative Translation Error (RTE) and Relative Rotation Error (RRE) compared to the baseline. This reflects a fundamental trade-off in dynamic scene perception. Explicitly filtering out dynamic regions successfully anchors the camera to a stable global environment, but it momentarily sacrifices the local signals used for relative frame-to-frame smoothness. This confirms our central hypothesis that establishing a globally superior static reference frame is the critical prerequisite for high-fidelity geometric reconstruction, even at the cost of short-term relative pose variance.

**Impact of Topological Subspace Surgery.** Adding the hard static replacement further refines the reconstruction, with additional reductions across all three principal metrics. The Accuracy Mean drops from 0.0282 to 0.0280, and the Distance Mean from 0.0531 to 0.0528. While these gains are more modest, they confirm that the topological surgery successfully prevents dynamic noise from corrupting the background geometry. As expected, the camera pose metrics remain largely unchanged during this geometry-focused stage.

**Table 2 Ablation study on the DyCheck dataset.** We progressively add each component and observe consistent improvement in the principal point cloud metrics (Acc Mean, Comp Mean, Dist Mean).

Configuration	Accuracy	Completeness	Distance	Pose Estimation		
	Mean ↓	Mean ↓	Mean ↓	ATE ↓	RTE ↓	RRE ↓
Baseline (VGGT4D)	0.0331	0.0962	0.0646	0.0183	<b>0.0100</b>	<b>0.3450</b>
+ Pose Decoupling	0.0282 (↓14.8%)	0.0779 (↓19.0%)	0.0531 (↓17.8%)	<b>0.0142</b> (↓22.4%)	0.0133 (↑33.0%)	0.5184 (↑50.3%)
+ Hard Replacement	<b>0.0280</b> (↓0.7%)	0.0775 (↓0.5%)	0.0528 (↓0.6%)	<b>0.0142</b>	0.0133	0.5181 (↓0.6%)
+ Conf. Fusion (Ours)	<b>0.0280</b>	<b>0.0751</b> (↓3.1%)	<b>0.0516</b> (↓2.3%)	<b>0.0142</b>	0.0114 (↓14.3%)	0.4406 (↓15.0%)

**Impact of Confidence-Aware Fusion.** Our final model, incorporating the information-theoretic confidence-aware fusion, achieves the best overall performance. It attains the lowest Completeness Mean (0.0751, a 3.1% reduction over the hard replacement variant) and Distance Mean (0.0516, a 2.3% reduction). By adaptively blending the multi-pass predictions based on uncertainty, the model smooths out localized errors that were rigidly preserved in the hard replacement variant. Additionally, this probabilistic formulation exhibits a positive regularizing effect on the overall trajectory evaluation, partially recovering RTE and RRE by 14.3% and 15.0% respectively compared to the preceding steps. The consistent improvement across all stages validates our progressive decoupling design. It demonstrates that exchanging a slight drop in relative pose smoothness for significant gains in global trajectory correctness and dense geometric fidelity is a highly effective strategy for 4D reconstruction.

## 5 Conclusion

In this paper, we presented a novel, training-free progressive decoupling framework for robust 4D scene reconstruction. By recognizing the fundamental tension between camera pose estimation and geometry modeling in dynamic scenes, we proposed a principled paradigm: stabilize the camera first, then stabilize the geometry. Through our Dynamic-Mask-Guided Pose Decoupling, Topological Subspace Surgery, and Information-Theoretic Confidence-Aware Fusion, we effectively isolate motion interference and optimally blend multi-pass geometric predictions. The mathematical formulation grounds our approach in the theory of Riemannian manifolds, orthogonal projections on Hilbert spaces, and Bayesian inference under heteroscedastic noise. Extensive evaluations demonstrate that our approach consistently improves the principal 3D point cloud geometric metrics over existing baselines. Our findings underscore the importance of explicit dynamic-static disentanglement and provide a principled mathematical foundation for adapting 3D foundation models to complex 4D environments.

## References

- [1] Gwangbin Bae, Ignas Budvytis, and Roberto Cipolla. Estimating and exploiting the aleatoric uncertainty in surface normal estimation. In Proceedings of the IEEE/CVF International Conference on Computer Vision, pages 13137–13146, 2021.
- [2] Yohann Cabon, Lucas Stofl, Leonid Antsfeld, Gabriela Csurka, Boris Chidlovskii, Jerome Revaud, and Vincent Leroy. Must3r: Multi-view network for stereo 3d reconstruction. In Proceedings of the IEEE/CVF Conference on Computer Vision and Pattern Recognition, pages 1050–1060, 2025.
- [3] Xingyu Chen, Yue Chen, Yuliang Xiu, Andreas Geiger, and Anpei Chen. Easi3r: Estimating disentangled motion from dust3r without training. In Proceedings of the IEEE/CVF International Conference on Computer Vision, pages 9158–9168, 2025.
- [4] Siyan Dong, Shuzhe Wang, Shaohui Liu, Lulu Cai, Qingnan Fan, Juho Kannala, and Yanchao Yang. Reloc3r: Large-scale training of relative camera pose regression for generalizable, fast, and accurate visual localization. In Proceedings of the Computer Vision and Pattern Recognition Conference, pages 16739–16752, 2025.
- [5] Xianze Fang, Jingnan Gao, Zhe Wang, Zhuo Chen, Xingyu Ren, Jiangjing Lyu, Qiaomu Ren, Zhonglei Yang, Xiaokang Yang, Yichao Yan, and Chengfei Lyu. Dens3r: A foundation model for 3d geometry prediction. arXiv preprint arXiv:2507.16290, 2025.
- [6] Hang Gao, Ruilong Li, Shubham Tulsiani, Bryan Russell, and Angjoo Kanazawa. Monocular dynamic view synthesis: A reality check. Advances in Neural Information Processing Systems, 35:33768–33780, 2022.
- [7] Lily Goli, Sara Sabour, Mark Matthews, Marcus A Brubaker, Dmitry Lagun, Alec Jacobson, David J Fleet, Saurabh Saxena, and Andrea Tagliasacchi. Romo: Robust motion segmentation improves structure from motion. In Proceedings of the IEEE/CVF International Conference on Computer Vision, pages 6155–6164, 2025.
- [8] Yu Hu, Chong Cheng, Sicheng Yu, Xiaoyang Guo, and Hao Wang. Vggt4d: Mining motion cues in visual geometry transformers for 4d scene reconstruction. arXiv preprint arXiv:2511.19971, 2025.
- [9] Alex Kendall and Yarin Gal. What uncertainties do we need in bayesian deep learning for computer vision? Advances in neural information processing systems, 30, 2017.
- [10] Bernhard Kerbl, Georgios Kopanas, Thomas Leimkühler, and George Drettakis. 3d gaussian splatting for real-time radiance field rendering. ACM Trans. Graph., 42(4):139–1, 2023.
- [11] Johannes Kopf, Xuejian Rong, and Jia-Bin Huang. Robust consistent video depth estimation. In Proceedings of the IEEE/CVF Conference on Computer Vision and Pattern Recognition, pages 1611–1621, 2021.
- [12] Yushi Lan, Yihang Luo, Fangzhou Hong, Shangchen Zhou, Honghua Chen, Zhaoyang Lyu, Shuai Yang, Bo Dai, Chen Change Loy, and Xingang Pan. Stream3r: Scalable sequential 3d reconstruction with causal transformer. arXiv preprint arXiv:2508.10893, 2025.
- [13] Vincent Leroy, Yohann Cabon, and Jérôme Revaud. Grounding image matching in 3d with mast3r. In European conference on computer vision, pages 71–91. Springer, 2024.

- [14] Zhengqi Li, Richard Tucker, Forrester Cole, Qianqian Wang, Linyi Jin, Vickie Ye, Angjoo Kanazawa, Aleksander Holynski, and Noah Snavely. Megasam: Accurate, fast and robust structure and motion from casual dynamic videos. In Proceedings of the IEEE/CVF Conference on Computer Vision and Pattern Recognition, pages 10486–10496, 2025.
- [15] Yuzheng Liu, Siyan Dong, Shuzhe Wang, Yingda Yin, Yanchao Yang, Qingnan Fan, and Baoquan Chen. Slam3r: Real-time dense scene reconstruction from monocular rgb videos. In Proceedings of the Computer Vision and Pattern Recognition Conference, pages 16651–16662, 2025.
- [16] Matteo Poggi, Filippo Aleotti, Fabio Tosi, and Stefano Mattocchia. On the uncertainty of self-supervised monocular depth estimation. In Proceedings of the IEEE/CVF conference on computer vision and pattern recognition, pages 3227–3237, 2020.
- [17] You Shen, Zhipeng Zhang, Yansong Qu, Xiawu Zheng, Jiayi Ji, Shengchuan Zhang, and Liujuan Cao. Fastvggt: Training-free acceleration of visual geometry transformer. arXiv preprint arXiv:2509.02560, 2025.
- [18] Zhenggang Tang, Yuchen Fan, Dilin Wang, Hongyu Xu, Rakesh Ranjan, Alexander Schwing, and Zhicheng Yan. Mv-dust3r+: Single-stage scene reconstruction from sparse views in 2 seconds. In Proceedings of the Computer Vision and Pattern Recognition Conference, pages 5283–5293, 2025.
- [19] Hengyi Wang and Lourdes Agapito. 3d reconstruction with spatial memory. In 2025 International Conference on 3D Vision (3DV), pages 78–89. IEEE, 2025.
- [20] Jianyuan Wang, Minghao Chen, Nikita Karaev, Andrea Vedaldi, Christian Rupprecht, and David Novotny. Vggt: Visual geometry grounded transformer. In Proceedings of the Computer Vision and Pattern Recognition Conference, pages 5294–5306, 2025.
- [21] Qianqian Wang, Yifei Zhang, Aleksander Holynski, Alexei A Efros, and Angjoo Kanazawa. Continuous 3d perception model with persistent state. In Proceedings of the Computer Vision and Pattern Recognition Conference, pages 10510–10522, 2025.
- [22] Shuzhe Wang, Vincent Leroy, Yohann Cabon, Boris Chidlovskii, and Jerome Revaud. Dust3r: Geometric 3d vision made easy. In Proceedings of the IEEE/CVF conference on computer vision and pattern recognition, pages 20697–20709, 2024.
- [23] Yuxi Xiao, Jianyuan Wang, Nan Xue, Nikita Karaev, Yuri Makarov, Bingyi Kang, Xing Zhu, Hujun Bao, Yujun Shen, and Xiaowei Zhou. Spatialtrackerv2: 3d point tracking made easy. arXiv preprint arXiv:2507.12462, 2025.
- [24] Kai Xu, Tze Ho Elden Tse, Jizong Peng, and Angela Yao. Das3r: Dynamics-aware gaussian splatting for static scene reconstruction. arXiv preprint arXiv:2412.19584, 2024.
- [25] Jianing Yang, Alexander Sax, Kevin J Liang, Mikael Henaff, Hao Tang, Ang Cao, Joyce Chai, Franziska Meier, and Matt Feiszli. Fast3r: Towards 3d reconstruction of 1000+ images in one forward pass. In Proceedings of the Computer Vision and Pattern Recognition Conference, pages 21924–21935, 2025.
- [26] David Yifan Yao, Albert J Zhai, and Shenlong Wang. Uni4d: Unifying visual foundation models for 4d modeling from a single video. In Proceedings of the Computer Vision and Pattern Recognition Conference, pages 1116–1126, 2025.
- [27] Junyi Zhang, Charles Herrmann, Junhwa Hur, Varun Jampani, Forrester Cole, Deqing Sun, and Ming-Hsuan Yang. Monst3r: A simple approach for estimating geometry in the presence of motion. In International Conference on Learning Representations, volume 2025, pages 82863–82886, 2025.
- [28] Songyan Zhang, Yongtao Ge, Jinyuan Tian, Guangkai Xu, Hao Chen, Chen Lv, and Chunhua Shen. Potato: Marrying pointmap matching with temporal motions for dynamic 3d reconstruction. In Proceedings of the IEEE/CVF International Conference on Computer Vision, pages 5680–5689, 2025.
- [29] Zhoutong Zhang, Forrester Cole, Zhengqi Li, Michael Rubinstein, Noah Snavely, and William T Freeman. Structure and motion from casual videos. In European Conference on Computer Vision, pages 20–37. Springer, 2022.
- [30] Kaichen Zhou, Yuhan Wang, Grace Chen, Xinhai Chang, Gaspard Beaudouin, Fangneng Zhan, Paul Pu Liang, and Mengyu Wang. Page-4d: Disentangled pose and geometry estimation for vgg-4d perception. arXiv preprint arXiv:2510.17568, 2025.